Will mercury impurities impact CO_2 injectivity in deep sedimentary formations? I. Condensation and net porosity reduction

Curtis M. Oldenburg

Nicolas Spycher

Earth Sciences Division

Lawrence Berkeley National Laboratory

September 10, 2014

This is the open-access version of the journal article. The citation for this work is:

Oldenburg, C.M. and Spycher, N., 2015. Will mercury impurities impact CO2 injectivity in deep sedimentary formations? I. Condensation and net porosity reduction. *Greenhouse Gases: Science and Technology*, *5*(1), pp.64-71. https://doi.org/10.1002/ghg.1472

ABSTRACT

Mercury is a common contaminant in natural gas and partially follows carbon dioxide through amine separation during natural gas processing. In this study, we used simple volumetric analyses, the simulator TOUGH2/EOS7C, and dew-point calculations to investigate the potential impacts on injectivity of trace amounts of mercury in a carbon dioxide stream injected for geologic carbon dioxide sequestration. For mercury concentrations up to 190 ppbV (~1.6 mg/stdm^3 CO_2), the total volumetric pore-space plugging that could occur around the wellbore due to complete condensation of mercury, or due to complete precipitation of mercury as cinnabar, results in a very small porosity change. Evaporative concentration of aqueous mercury by water evaporation into carbon dioxide is unlikely because the volatility of mercury into the carbon dioxide stream is higher than that of water. Dew-point calculations suggest that mercury concentrations of about 2,000 ppbV are needed for mercury condensation to occur. Our analyses suggest that for mercury concentrations of a few hundred ppbV, the impacts on injectivity of mercury deposition by condensation or precipitation as cinnabar are negligible.

1 Introduction

Minimum standards for heating value of produced gas (mostly methane, CH_4) from natural gas reservoirs often necessitate processing of the natural gas to remove carbon dioxide (CO_2) and other constituents before the gas is sent to market. By the process of amine absorption during natural gas processing, large amounts of CO_2 may be separated from the natural gas, and in some cases re-injected for geologic carbon dioxide sequestration (GCS). For example, gas processing has resulted in the total sequestration of approximately 18 Mt CO_2 (1.8×10^{10} kg CO_2) at Sleipner [1],

2 Mt CO_2 at Snovhit [2], and 7 Mt CO2 at In Salah [3]. Another common contaminant in natural gas is mercury (Hg) [4, 5]. While Hg concentrations are not an issue in the three aforementioned natural gas fields, Hg concentrations may be higher in future high-CO_2 natural gas projects involving GCS, and a fraction of the Hg present in the natural gas may be captured along with CO_2 (e.g. [6] and potentially injected for GCS. Even though Hg may range from trace concentrations up to hundreds of ppbV as assumed in this study, enormous volumes of the CO_2-Hg injectate will be sent down wells for sequestration. While other studies have considered reduction in injectivity due to effects of various contaminants (e.g., [5]), we are not aware of studies directed at Hg and particularly pore plugging by condensation and/or mineral precipitation of Hg-bearing minerals. Here we address the question of whether Hg in the CO_2 injection stream can negatively impact injectivity (defined as bottomhole pressure rise per unit mass of CO_2 injected) by reducing permeability in the geologic formation.

Trace amounts of Hg in large volumes of injected CO_2 could reduce injectivity in at least two ways. First, the condensation of Hg (vapor depositing in the pore space as liquid) could reduce the CO_2 relative permeability in the formation. In addition, the precipitation of Hg-containing minerals such as cinnabar (HgS) could reduce porosity of the formation, with associated effects on permeability. In this study, we present simple volumetric calculations, numerical modeling, and equilibrium dew-point analyses to investigate whether Hg condensation or precipitation of Hg as cinnabar can be expected to reduce injectivity substantially. In a companion paper [7], we present detailed geochemical modeling of reactions caused by the injected CO_2 and Hg that could lead to the dissolution and precipitation of other (non-Hg) minerals, as well as Hg-containing mineral phases, which could possibly affect injectivity arising from Hg injection.

2 Methods

In this study, we present simple volumetric analyses, idealized numerical simulations, and dew-point calculations to evaluate potential pore-occupancy and evaporation-condensation processes of Hg injected as a trace contaminant with a CO_2 carrier gas into an idealized saturated porous media reservoir formation at a depth of approximately 2 km (~210 bar, 106 ºC). The volumetric calculations, which assume that a cylindrical porous region around the wellbore is uniformly permeated with injected CO_2 and Hg, were made to evaluate the amount and volume of Hg injected with CO_2 and to assess the effects on porosity of different volumetric distributions of Hg and CO_2 within the target formation.

Dynamic changes in aqueous Hg concentration were investigated by numerical simulation using TOUGH2/EOS7C to simulate the evaporative concentration behavior of trace soluble gas species (such as Hg) of different volatilities. TOUGH2 is a multiphase and multicomponent integral finite difference reservoir simulator [8, 9] is an equation of state module for TOUGH2 that calculates thermophysical properties of H_2O, brine, non-condensible gas (e.g., CO_2), gas tracer, CH_4 under (optional) non-isothermal conditions. The Peng-Robinson (cubic) equation of state is used in EOS7C to calculate gas mixture fugacity, density, enthalpy departure, and viscosity. Equilibrium gas solubility is computed using a Henry's Law approach. For applications in this study, we set the CH_4 concentration to be negligible, and we made the tracer component represent the volatile Hg component by specification of concentration and Henry's Law constant to values appropriate for Hg for the given *P*-*T* conditions in the reservoir (see Appendix A).

As confirmation of the numerical simulations, and to extend the analysis to estimate effects of higher Hg concentrations, equilibrium thermodynamic dew-point calculations were performed to assess the potential for gaseous Hg (in the CO_2) to condense from the CO_2.

3 Results

3.1. System properties

Relevant properties and operational parameters of a hypothetical GCS reservoir and injectate composition are shown in Table 1. As shown, we consider CO_2 with 190 pbbV Hg will be injected at a rate of 0.47 Mt/yr for 40 yrs into a well with 300 m of screened interval. The scope of this project involved choosing a set of properties typical of prospective GCS sites to investigate expected effects, leaving for later the assessment as to whether future studies, including exhaustive calculations of ranges of properties, are warranted. All results are calculated and presented on a per well basis.

96 ***Table 1.*** *Property, operational, and reference data*

Variable	Value	Units	Source
Pressure	215	(bar)	1
Temperature	106	(C)	1
Porosity	0.15		1
Residual CO_2 saturation	0.4		1
Thickness of injection interval	300	(m)	2
CO_2 injection rate per injector	2.53E+08	(std m^3/y)	1
	14.8	(kg/s)	1
Injection time period	40	(y)	1
Hg concentration in CO_2	1.58	(mg/m^3)	1
	0.19	(ppmV)	1
CO_2 density (reservoir, 215 bar, 106°C)	490.5	(kg/m^3)	2
Hg(l) density (1 bar, 20°C)*	13,546	(kg/m^3)	3
HgS(s) density (1 bar, 25°C)*	8,176	(kg/m^3)	5
CO_2 molecular weight	44.0095	(g/mol)	4
Hg(l) molecular weight	200.59	(g/mol)	4
HgS(s) molecular weight	232.66	(g/mol)	4

97 * Minimal temperature and pressure effects are neglected
98 Source: 1 assumption; 2 Altunin (1975) [10]; 3 Holman and ten Seldam (1994) [11]; 4 NIST (2011) [12]; 5
99 Mindat.org (http://www.mindat.org/min-1052.html, last accessed 12/12/2013).

100

101 **3.2. Hg Effect on Porosity**

102 The maximum porosity change from Hg deposition in a reservoir can be estimated by simple
103 volumetric analyses, assuming that all of the available Hg either condenses or precipitates as
104 cinnabar (HgS(s)) within a uniform cylindrical volume around the wellbore.

105 Approximate volumes of injected CO_2 and Hg were calculated using injection conditions and
106 assumptions of Tables 1 and 2. For these simple analyses, it is assumed that all Hg initially in the
107 CO_2 is deposited in the target formation, either as condensed elemental liquid mercury (Hg(l)) or
108 as precipitated cinnabar (mercury sulfide, HgS(s)), which is known to readily form in the presence
109 of sulfide (e.g., [13] and has an extremely low solubility [14, 15]).

The calculated Hg mass flow rate into the target formation is 400 kg/y (Table 2). However, the corresponding (maximum) volumes of Hg or cinnabar that could condense and precipitate (respectively) upon injection are 1.18 and 1.95 m^3, respectively, a very small volume relative to the huge volume of injected supercritical CO_2. This is the result of the high densities of Hg(l) and HgS(s) relative to the density of supercritical CO_2 at reservoir pressure and temperature. Note that the change in Hg(l) and HgS(s) density with temperature and pressure is negligibly small and therefore neglected (e.g., [11]). Given these small expected volumes, it is evident that a significant reduction in permeability from Hg deposition would only arise if deposition (by either condensation or precipitation) occurred within the pore space of a small and localized region of the reservoir.

If we assume that Hg deposition by either condensation (as Hg(l)) or precipitation (as HgS(s)) occurs uniformly around 300 m of the 0.25 m (10-inch) injection well, it is possible to roughly estimate the lateral extent of Hg deposition around the well versus porosity drop, or vice versa. In doing so, it is estimated that an absolute porosity drop of more than 1% would require precipitation of all of the injected Hg within less than ~0.2–0.4 m from the injection well (Figure 1). If, on the other hand, Hg deposition occurred over meters to tens of meters as we might intuitively expect, the porosity drop would be correspondingly smaller, as would the impact on porosity and therefore on injectivity. While this simple analysis does not consider the details of where deposition might occur, e.g., in pore throats versus within pore bodies, the small volume of Hg available to reduce porosity suggests minimal effects on injectivity.

We note that the numerical simulations presented in the companion paper [7 reveal that the distribution of CO_2 and Hg around the injection well cannot be assumed to be cylindrical in shape

132 because the buoyancy of supercritical CO_2 results in an upward-widening conical plume around
133 the wellbore. Regardless of this buoyancy complication, the simple volumetric calculations
134 considered here suggest that a very small porosity change would occur if Hg precipitated in a
135 distributed fashion over length scales of a meter or more around the well. Additional studies
136 focused on leakage and CO_2 permanence will have to be carried out to address the question of the
137 ultimate fate of Hg dissolved in the CO_2 phase. We show in the companion paper [7] that Hg
138 readily precipitates as cinnabar (HgS) (because sulfide is present in formation waters) and that this
139 mineral has an extremely low solubility, meaning that significant Hg contamination of reservoirs
140 is not expected.

141 ***Table 2.*** *Approximate Hg and CO_2 volumetric data calculated using assumptions and data shown in*
142 *Table 1.*

Variable	Value	Units
Hg mass and volumetric rates[1]		
Mass rate	399	(kg/y)
Volumetric rate as Hg(l)	0.0295	(m^3/y)
Volumetric rate as HgS(s)	0.0489	(m^3/y)
Cumulative volumetric data[1,2]		
Reservoir volume with residual CO_2	6.35E+08	(m^3)
Total Hg volume as Hg(l)	1.18	(m^3)
Total Hg volume as HgS(s)	1.95	(m^3)
Radius of CO_2 plume	821	(m)

143 [1]Per injector; [2]Assuming a cylindrical plume centered on the injector at residual saturation shown.
144

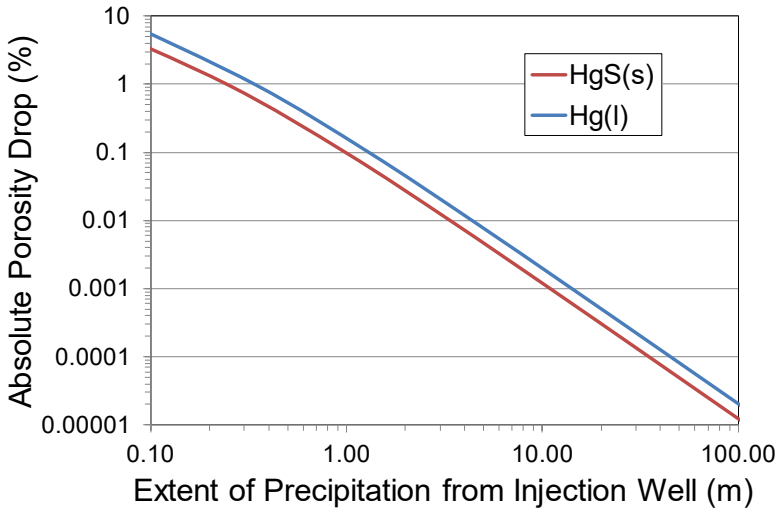

Figure 1. *Absolute porosity change estimated for a given extent of homogeneous Hg deposition radially around an injector well (see Tables 1 and 2 for assumptions and inputs).*

3.3. Evaporative Concentration

To the extent that the above analyses hinge on the total volume of Hg, and therefore on the concentration of Hg in the gas or aqueous phases, the question arises as to whether Hg could concentrate in the residual aqueous phase of the formation as CO_2 absorbs H_2O from resident groundwater. For example, small quantities of water are known to evaporate into compressed CO_2, resulting in evaporative concentration of dissolved salts and in some cases reduction in formation permeability (e.g., [16, 17, 18]). Therefore, could aqueous Hg also condense or precipitate as cinnabar during continued drying, causing significant reductions in porosity? (Note that the effects of water evaporation on the precipitation of other minerals is negligible in this case [7].

To motivate the question further, we consider three examples of this potential effect. Specifically, we imagine three idealized beakers containing aqueous mixtures with solutes (NaCl, CH_4, and Hg) of different volatility. When H_2O evaporates from the beaker containing the NaCl solution, NaCl concentrates because it does not volatilize. In the beaker containing dissolved CH_4, the CH_4 volatilizes faster than H_2O resulting in lower concentration of CH_4 in the solution as time goes on. What about the beaker containing dissolved Hg? Does Hg concentrate or diminish as evaporation into a dry CO_2 stream occurs?

To demonstrate and verify the behavior of Hg upon continuous CO_2 injection, a simple numerical experiment was set up to simulate the evaporation of different solutions, each containing a dissolved (generic) compound with a given different volatility. The numerical experiment examines the evolution of Hg concentration in the aqueous phase upon evaporation of H_2O into a through-flowing CO_2 stream at 213 bars and 106°C. Three grid blocks were defined as shown in Figure 2. Dry CO_2 is injected into the first grid block, which is initially filled with a small amount of aqueous phase that quickly dries up. This CO_2 flows directly into the second grid block that contains a two-phase mixture of gas and aqueous phase, where the aqueous phase contains Hg at a concentration of 5.6×10^{-8} by mass fraction (approximately the solubility of Hg estimated for the reservoir of interest). In this second grid block, instantaneous equilibrium concentrations of H_2O, CO_2, and Hg in the gas and aqueous phases are calculated. The gas phase from grid block 2 then flows into the third grid block which is an effective sink for whatever phases and components flow into it. The question we have posed can be answered by simply monitoring the aqueous phase

concentration in the second grid block; in short, does Hg concentration increase or decrease as CO_2 flows through?

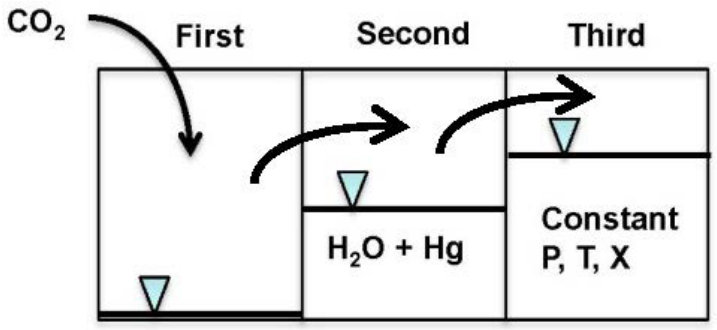

Figure 2. *Sketch of the three grid blocks used to model the evolution of Hg concentration in the aqueous phase of the second grid block as dry CO_2 flows through it.*

Simulations were carried out using TOUGH2/EOS7C considering a tracer with various assigned values of Henry's Law constant (*Kh*). In doing so, systems representative of Hg, as well as hypothetical more- and less-volatile components, could be modeled. The *Kh* values for Hg at the temperature and pressure of interest was estimated to be about 8.2×10^8 Pa/mole fraction (Appendix A).

Results are shown in Figure 3 by curves of gas saturation (left-hand side vertical axis) and Hg concentration (mass fraction in the aqueous phase) in the second grid block, computed for various values of $1/Kh$. The gas saturation is predicted to increase steadily as the H_2O component evaporates from the aqueous phase. For Hg (at $1/Kh \sim 1.22 \times 10^{-9}$ Pa^{-1}; solid blue curve), the Hg concentration is computed to rapidly decline with time, indicating that Hg will not concentrate in the aqueous phase as CO_2 flows through. Additional results for hypothetical solutes with various

198 1/*Kh* values are shown in Figure 3. For 1/*Kh* values larger than 7.994×10^{-6} Pa^{-1}, the solute
199 concentrates as evaporation occurs. This critical value of 1/*Kh*, separating concentrating from
200 non-concentrating solutes, subject to contact with dry CO_2, represents the inverse of the
201 saturation pressure of water at the considered *P*-*T* conditions. In other words, if a solute is more
202 volatile than water in the CO_2 stream, its concentration will decrease in the aqueous phase as
203 drying occurs. If the solute is less volatile than water, its concentration will increase. This result
204 shows that the concentration of Hg in a two-phase groundwater-gas region is expected to
205 decrease as CO_2 flows through, because the Hg component is more volatile (by several orders of
206 magnitude) than the H_2O component into the CO_2 stream. This behavior implies that Hg will
207 tend to be transported farther into the formation with the flowing CO_2 rather than accumulating
208 around the near-well region where it could impact injectivity. Because the gas phase in the
209 second grid block will contain H_2O at its saturation limit after instantaneous equilibrium, the
210 qualitative behavior does not depend on whether CO_2 injected into this grid block is initially dry
211 or partially saturated with H_2O. In short, the greater volatility of Hg ensures that it preferentially
212 enters the gas phase relative to H_2O.

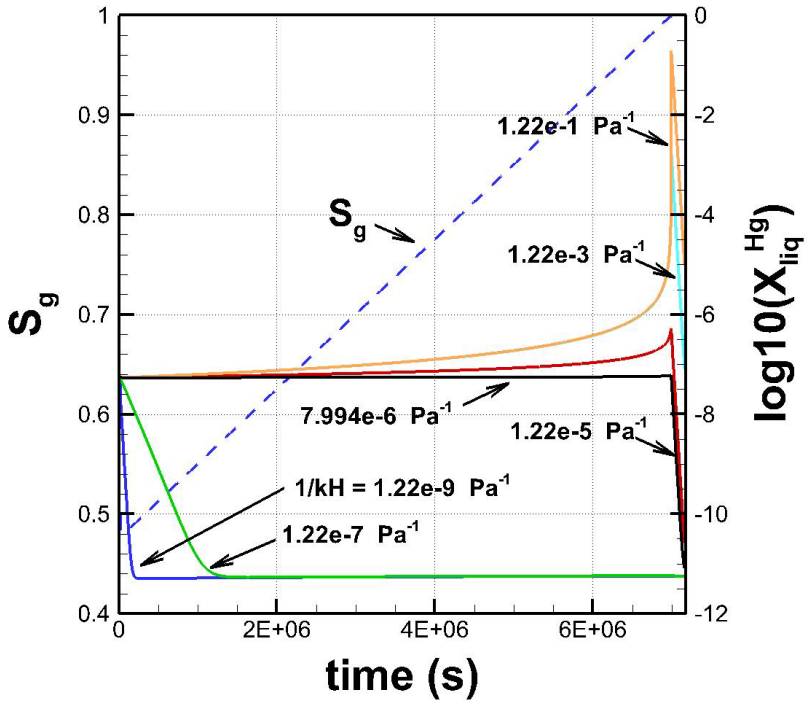

Figure 3. *TOUGH2/EOS7C results of gas saturation (S_g) and log mass fraction of Hg in the liquid (aqueous) phase as a function of time in the second grid block for solutes with various 1/Kh values. The curve for Hg is shown by the blue solid line (1/Kh = 1.22 × 10^{-9} Pa^{-1}). Note that the sharp curve reversals near the right axis are caused by the aqueous phase drying up after 7 × 10^6 s (81 day)s.*

3.4. Hg Condensation potential

The potential for Hg condensation from the supercritical CO_2 phase as Hg(l) (liquid elemental mercury) was investigated by applying simple dew-point calculations, using Hg vapor-pressure data from the literature (Appendix A). The potential for Hg(l) condensation from the supercritical CO_2 phase can be estimated in a manner analogous to the calculation of air relative humidity. The "relative humidity" of Hg in CO_2, under ideal conditions, can be expressed by

$$RH = P_{Hg}/P_{satHg} = y_{Hg}\, P_{tot} / P_{satHg} \qquad (1)$$

where *RH* stands for "relative humidity", P_{Hg} is the partial pressure of Hg in the CO_2, P_{satHg} is the saturation pressure of Hg, P_{tot} is the total system pressure, and y_{Hg} is the mole fraction of Hg in CO_2. The concentration of Hg in the gas phase required for condensation to occur (i.e., the saturation concentration) can be estimated by setting *RH* equal to 1 in Eq. 1 (to express saturation), and solving for y_{Hg} given the Hg vapor pressure (~51×10^{-5} bar at 106°C; Appendix A) and the total system pressure. These calculations for the total system pressure of 213 bar show that an Hg concentration ten times higher (> 2,000 ppbV) than the concentration considered here (~190 ppbV) would be required for condensation to occur (Figure 4).

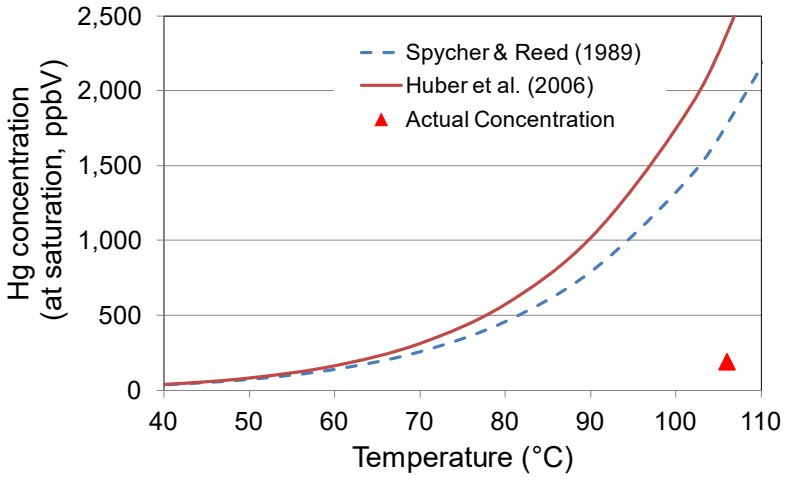

Figure 4. *Hg saturation concentration at 213 bar (assuming ideal gas behavior; see Appendix A). The actual Hg concentration is significantly below the saturation level.*

4 Conclusions

A series of simple analyses was carried out to assess the potential for Hg to impact injectivity through condensation (Hg(g) to Hg(l)) or precipitation as cinnabar from a stream of Hg-containing supercritical CO_2 injected into a geologic formation at 213 bar and 106°C. The simple modeling

analyses suggest that the co-injection of small quantities of Hg (up to 190 ppbV) with CO_2 into a deep geologic formation are not expected to significantly impact injectivity through condensation or precipitation. The results suggest further that evaporative concentration of Hg will not occur because of the high volatility of Hg relative to H_2O. Concentrations of Hg higher than ~2,000 ppbV at the *P-T* conditions modeled could potentially lead to condensation of gaseous Hg to Hg(l), which could affect the relative permeability of the injected CO_2 stream. Detailed reactive geochemical modeling of Hg reactions in a generalized sandstone reservoir are presented in a companion paper [7].

We emphasize that the results presented here are general and theoretical in nature, relying on models, assumptions, and various data that have an inherent uncertainty and/or variability. As such, the results should be regarded as more qualitative than quantitative. Site-specific modeling and simulation will be needed to assess actual Hg deposition processes and impacts to injectvity in individual cases.

5 Acknowledgements

We thank Tim Kneafsey (LBNL) for helpful discussions and review of an earlier draft. Support for this work was provided by Chevron with project management by Scott Imbus (Chevron). Additional support was provided by the Assistant Secretary for Fossil Energy (DOE), Office of Coal and Power Systems, through the National Energy Technology Laboratory (NETL), and by Lawrence Berkeley National Laboratory under Department of Energy Contract No. DE-AC02-05CH11231.

6 References

1) Chadwick A, Williams G, Delepine N, Clochard V, Labat K, Sturton S, Buddensiek M-L, et al., Quantitative analysis of time-lapse seismic monitoring data at the Sleipner CO_2 storage operation, *The Leading Edge* 29(2), 170-177 (2010).
2) Shi J-Q, Imrie C, Sinayuc Cr, Durucan S, Korre A, and Eiken O, Snøhvit CO_2 Storage Project: Assessment of CO_2 Injection Performance Through History Matching of the Injection Well Pressure Over a 32-months Period, *Energy Procedia* 37, 3267-3274 (2013).
3) Ringrose P, Atbi M, Mason D, Espinassous M, Myhrer Ø., Iding M., Mathieson A, and Wright I, Plume development around well KB-502 at the In Salah CO2 storage site, *First Break* 27(1) (2009).
4) Bingham MK, Field detection and implications of Mercury in natural gas. *SPE Production Engineering,* May 1990, 120-124 (1990).
5) IEAGHG, "Effects of impurities on geological storage of CO_2," 2011/04 June (2011).
6) Cui Z, Aroonwilas A, and Veawab A, Simultaneous capture of mercury and CO_2 in amine-based CO_2 absorption process, *Industrial & Engineering Chemistry Research* 49.24: 12576-12586 (2010).
7) Spycher N, and Oldenburg CM, Will mercury impurities impact CO_2 injectivity in deep sedimentary formations? II. Mineral dissolution and precipitation, *Greenhouse Gases: Sci. and Tech.*, companion paper, submitted (2014).

8) Pruess K, Oldenburg CM, and Moridis GJ. TOUGH2 User's Guide Version 2.1. E. O. Lawrence Berkeley National Laboratory Report LBNL-43134, 1999; and LBNL-43134 (revised) 2012.

9) Oldenburg CM, Moridis GJ, Spycher N, and Pruess K, EOS7C Version 1.0: TOUGH2 Module for Carbon Dioxide or Nitrogen in Natural Gas (Methane) Reservoirs, Lawrence Berkeley National Laboratory Report *LBNL-56589*, March (2004).

10) Altunin VV, Thermophysical properties of carbon dioxide. Moscow: Publishing House of Standards, 551 pp. (in Russian) (1975).

11) Holman GJF, ten Seldam CA, A critical evaluation of the thermophysical properties of mercury. *J. Phys. Chem. Ref. Data*, 23, 5, 807-827 (1994).

12) NIST NIST Chemistry Web Book, NIST Standard Reference Database Number 69, June (2011) Release [online]: http://webbook.nist.gov/chemistry.

13) Audeh CA Hydrogen sulfide: an effective reagent for reducing the elemental mercury content of liquid hydrocarbons. ACS Division of Fuel Chemistry, preprints of papers presented at the 206th ACS National Meeting, Chicago, 1993, Aug 22-26, 38 No. 3, 787-974 (1993).

14) Schwarzenbach G; Widmer M, Die loslichkeit von metallsulfiden I. Schwarzes quecksilbersulfid. Helv. Chim. Acta 1963, 46, 2613−2628 (1963).

15) Paquette KE, Helz GR, Inorganic speciation of mercury in sulfidic waters: The importance of zerovalent sulfur. Environ. Sci. Technol., 31, 2148-2153 (1997).

16) Pruess K, Müller N, Formation dry-out from CO_2 injection into saline aquifers: 1. Effects of solids precipitation and their mitigation. *Water Res. Research*, 45, W03402, doi:10.1029/2008WR007101, (2009).

17) Borgia A, Pruess K, Kneafsey TJ, Oldenburg CM, and Pan L, Numerical simulation of salt precipitation in the fractures of a CO_2-enhanced geothermal system, *Geothermics*, *44*, 13-22 (2012).

18) Kim, KY, Han WS, Oh J, Kim T, and Kim J-C, Characteristics of salt-precipitation and the associated pressure build-up during CO2 storage in saline aquifers." *Transport in Porous Media 92*, no. 2, 397-418 (2012).

19) Huber ML, Laesecke A, Friend DG The Vapor Pressure of Mercury. Report NISTIR 6643, National Institute of Standards and Technology, Boulder, CO 80305-3328, 56 pp, (2006).

20) Spycher NF, Reed MH, Evolution of a Broadlands-type epithermal ore fluid along alternative P-T paths: implications for the transport and deposition of base, precious, and volatile metals. *Economic Geology*, 84, 328-359 (1989).

21) Andersson ME, Gårdfeldt K, Wängberg I, and Strömberg D, Determination of Henry's law constant for elemental mercury. *Chemosphere*, 73, 587–592 (2008).

22) Wagner W, Pruss A, The IAPW formulation 1995 for the thermodynamic properties of ordinary water substance for general scientific use. *J. Phys. Ref. Data,* **31**, 387–535 (2002).

Appendix A – Hg vapor pressure and Henry's Law constant

Huber et al. (2006) [19] presented a correlation to compute the Hg vapor pressure as a function of temperature, which they fitted to a large number of experimental data points from the literature. The results of this correlation were compared to Hg vapor pressures computed from equilibrium constants (as a function of temperature) for the reaction Hg(v) ↔ Hg(l), derived by Spycher and Reed (1989) [20] using published Gibbs free energy data. These compare reasonably well at low temperatures with Huber et al. (2006) [19], but deviate at higher temperatures (Figure A1), reflecting the variability in published experimental data.

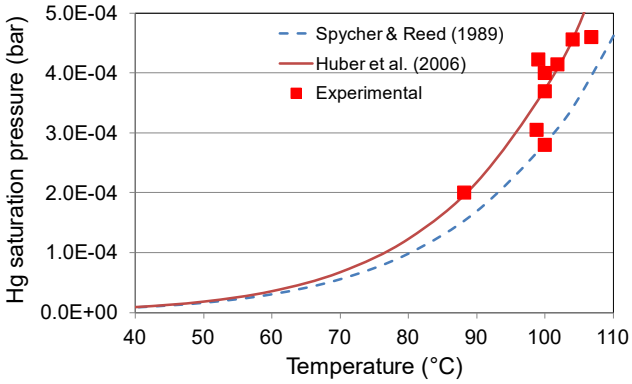

Figure A1. *Hg saturation pressure as a function of temperature. Symbols show a few of the experimental data points compiled by Huber et al. (2006) in the range 90–110°C.*

Henry's Law constant (*Kh*) values for Hg were derived using data for equilibrium constants as a function of temperature for the reaction Hg(v) ↔ Hg(aq) reported by [20] Spycher and Reed (1989). These data were not corrected for pressure, but the pressure effect on *Kh* was evaluated

by applying a Poynting factor, calculated using an average molar liquid Hg volume estimated from the molecular weight and density data shown in Table 1. This factor yields a decrease in Hg solubility by about 10% at 106°C and 215 bar (Figure A2). Therefore, neglecting the pressure effect tends to overestimate the solubility of Hg, which then would underestimate the potential for condensation. However, the gaseous Hg concentrations considered here are below the saturation limits by a factor of at least 10 (Figure 4), which is much greater than the 10% decrease in solubility caused by the pressure correction. Therefore this pressure effect does not affect the conclusions reached in this study. Original and pressure-corrected *Kh* values for Hg compare favorably to the *Kh* values reported in [12] and [21] (Figure A2). This figure also shows the saturation pressure curve of pure water from [22] for comparison.

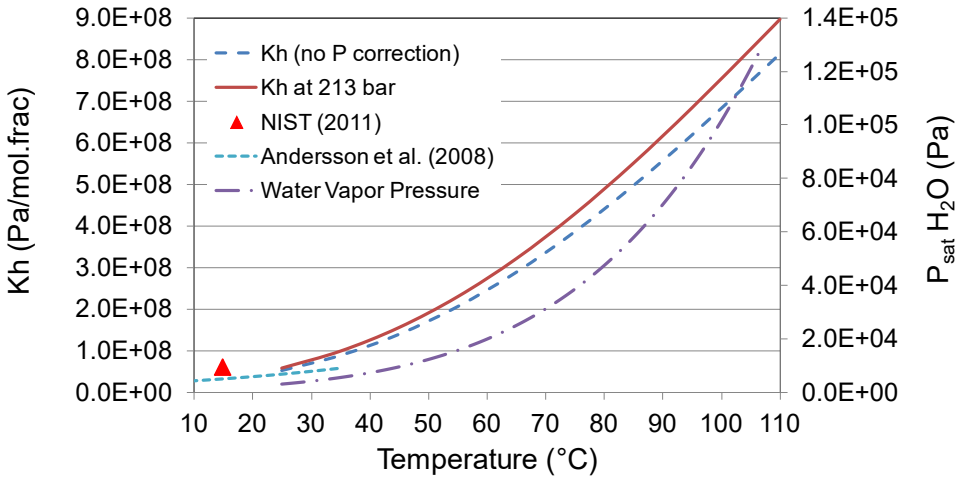

Figure A2. *Estimated Henry's law constant for Hg (Kh) (left-hand side axis) and water vapor saturation pressure (right-hand side axis) versus temperature.*